Efficient Synthesis and Electronic Studies of Core−Shell Nanowires Based on Colossal Magnetoresistive Manganites

Bo Lei, Chao Li, Daihua Zhang, Song Han, and Chongwu Zhou*

Departments of Electrical Engineering and Electrophysics, University of Southern California, Los Angeles, California 90089

Received: June 21, 2005; In Final Form: July 30, 2005

We report our recent study on the pulsed laser deposition process in the synthesis of colossal magnetoresistive $MgO/LaCaMnO_3$ and $MgO/LaSrMnO_3$ core−shell nanowires. A highly efficient process has been developed by depositing an epitaxial layer of manganite onto randomly oriented MgO nanowires grown on SiO_2/Si substrates. In addition, in-depth studies revealed that the sample−target distance played a critical role in determining the core−shell nanowire quality. The $MgO/LaCaMnO_3$ and $MgO/LaSrMnO_3$ nanowires opened up the unique opportunity to explore a number of intriguing physical properties at the nanoscale. Remarkable metal−insulator phase transitions and pronounced colossal magnetoresistance have been observed in both $LaCaMnO_3$ and $LaSrMnO_3$ nanostructures.

Interests in one-dimensional (1-D) heteronanostructures stem from their promising potential as unique types of nanoscale building blocks for larger superstructures that can be applied in a variety of applications. In particular, 1-D coaxial layered nanostructures with modulated composition and interfaces have attracted considerable attention recently.[1−14] A primary and versatile synthetic approach to such core−shell nanocables is to coat conformal sheaths made of different materials onto existing 1-D nanotemplates, namely, nanowires, nanoribbons, or nanobelts using various techniques including chemical vapor deposition (CVD),[1,2] arc discharge,[3] pulsed laser deposition (PLD),[4−6] and wet chemical methods.[7−10] Among them, the PLD technique demonstrates unique advantages over other methods in processing complex compounds, which provides an easy and generic approach to producing stoichiometric and epitaxial coatings. However, in sharp contrast to 2-D thin films,[15−19] research on this powerful technique in the synthesis of 1-D heterostructures is still in a preliminary stage despite successful previous efforts.[4−6] We herein report our systematic study on the PLD process using both vertically aligned and randomly orientated $MgO/La_{1-x}A_xMnO_3$ (X = 1/3, A = Ca, Sr) core−shell nanowires as sample models. In addition to their synthetic simplicity, the two materials were selected based on, more importantly, their scientific and technological importance.

Mixed-valence manganese oxides (manganites) such as $La_{0.67}Ca_{0.33}MnO_3$ (LCMO) and $La_{0.67}Sr_{0.33}MnO_3$ (LSMO) possess a wide collection of intriguing electronic and magnetic properties.[20−24] Driven by their potential applications in diverse areas including magnetic recording,[25,26] bolometric application,[27] spin-valve devices, and vertical tunneling magnetoresistance (TMR) junctions, [28] considerable research has been devoted to the synthesis and characterization of manganites in both bulk and thin film forms.[29−31] However, investigations on the manganite-based nanostructures such as 1-D nanowires [32] and 0-D nanocubes [33] have been rarely reported despite their unique potential applications (e.g., high-density magnetic data storage) and substantial scientific merits in fundamental studies. In this context, we have carried out intensive research on manganite nanostructures and successfully synthesized single crystalline MgO/LCMO and MgO/LSMO core−shell nanowires by depositing epitaxial LCMO or LSMO sheaths onto MgO nanowire templates through the PLD technique. These novel nanostructures opened up the unique opportunity to explore a number of intriguing physical properties such as metal−insulator phase transitions and colossal magnetoresistance (CMR) at the nanoscale.

This paper will focus on both our in-depth investigation of the newly developed PLD technique as well as our systematic studies on the electron transport behavior in 1-D LCMO and LSMO nanostructures. We have developed an efficient way to synthesize both LCMO and LSMO nanowires by using MgO nanowires grown on Si/SiO_2 substrates as the template for subsequent PLD. Following the material synthesis, a series of material characterizations and electronic transport studies have been conducted. Remarkable metal-to-insulator transition (MIT) was observed in both LCMO and LSMO core−shell nanowires. Such 1-D manganite nanostructures also exhibited pronounced magnetoresistance around the transition temperature (T_{MIT}), which was calculated as ∼34 and ∼12% at $B = 2$ T for LCMO and LSMO nanowires, respectively.

Our experiments started from the preparation of LAMO (A = Ca, Sr) targets and MgO nanowire templates. LAMO has a cubic perovskite structure with a lattice constant of $a_{LCMO} = 3.87$ Å and $a_{LSMO} = 3.89$ Å (upper part of Figure 1b). [21] In each unit cell, the trivalent La and A divalent ions occupy the eight corners, while the Mn ion sits at the center of the octahedron formed by six oxygen atoms at the cubic face centers. In our study, the LAMO target was made by compressing $La_{0.67}Ca_{0.33}MnO_3$ or $La_{0.67}Sr_{0.33}MnO_3$ powders (SCI Inc.) into a circular disk followed by postsintering at 1000 °C in ambient air for 10 h. The MgO nanowire shares a very similar lattice structure with LAMO, with a slightly larger lattice constant of $a_{MgO} = 4.21$ Å[21] (lower part of Figure 1b). The vertically aligned and randomly oriented nanowires were grown on single-crystalline MgO (100) substrates and Si/SiO_2 substrates, respectively, following the thermal CVD approach

* Corresponding author. E-mail: chongwuz@usc.edu.

10.1021/jp053334p CCC: $30.25
Published on Web 09/17/2005

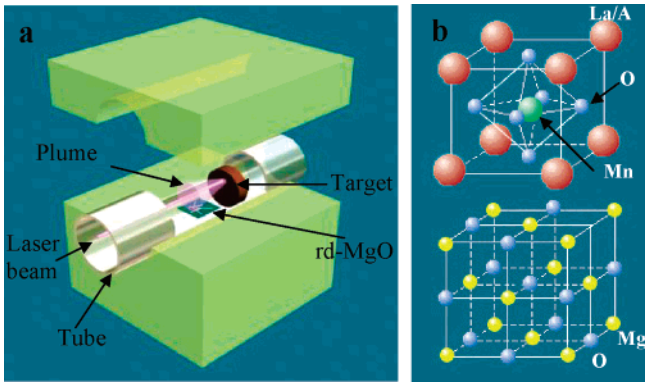

Figure 1. (a) Schematic diagram of the pulsed laser deposition system used to grow MgO/LCMO and MgO/LSMO core−shell nanowires. (b) Upper figure: a unit cell of mixed-valence manganite with a cubic perovskite structure and lower figure: a unit cell of MgO with a rock salt (cubic) structure. Here La/A (A = Ca, Sr), Mn, Mg, and O are indicated as orange, green, yellow, and blue, respectively.

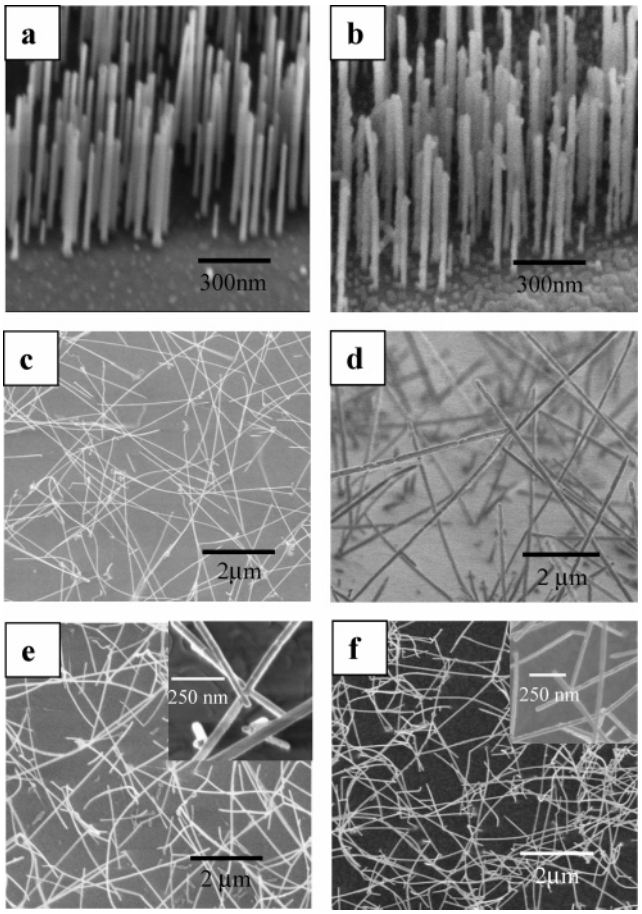

Figure 2. SEM images of (a) vertical MgO nanowires and (b) MgO/LCMO core−shell nanowires grown on a single crystalline (100) MgO substrate. (c) Top view and (d) perspective view of randomly oriented MgO nanowires on a Si/SiO_2 substrate. (e) SEM images of MgO/LCMO and (f) MgO/LSMO core−shell nanowires grown on a Si/SiO_2 substrate. Insets of panels e and f: SEM images of MgO/LCMO and MgO/LSMO core−shell nanowires showing a smooth nanowire surface after coating.

reported previously.[5] The LAMO shell layer deposition was performed in a PLD system consisting of a tube furnace and a solid-state Nd:YAG laser (Figure 1a). The target was mounted at the center of the tube furnace with the MgO nanowire sample positioned 0.5−4 cm away. The tube was prepumped to ~1.0×10^{-3} Torr and then pressurized with oxygen to the targeting pressure (200 mTorr for LCMO and 350 mTorr for LSMO)

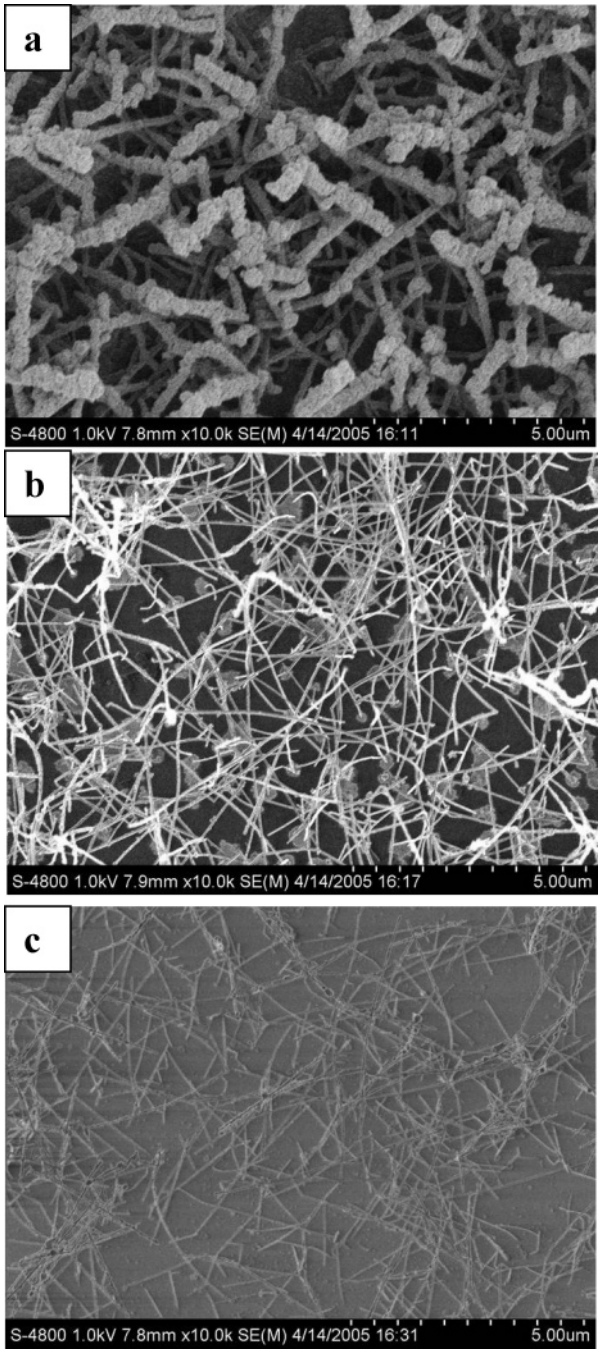

Figure 3. SEM images of MgO/LSMO nanowires on a Si/SiO_2 substrate taken from a sample placed at a different target-to-substrate distance, with D = 0.5, 2, and 4 cm for panels a−c, respectively.

before the deposition. The temperature and oxygen flow rate were maintained at 800 °C and 16 sccm during the LAMO growth. A frequency-doubled laser beam (532 nm) was used to ablate the manganite target with a repetition rate of 10 Hz and power density of 300 mW/cm^2 calculated at the focus plane (the direction is opposite to the gas flow). We have estimated the deposition rate as 1−2 Å/min. A growth time of 80 min was typically used to obtain a 10 nm thick shell layer. The PLD system was gradually cooled to room temperature with a ramping rate of 15 °C/min after the deposition was completed.

The SEM images of the nanowires before and after coating are shown in Figure 2. The vertically aligned bare MgO nanowires appear straight and well-separated on the single crystalline MgO substrate (Figure 2a). After the LCMO deposition, most of MgO/LCMO core−shell nanowires remained

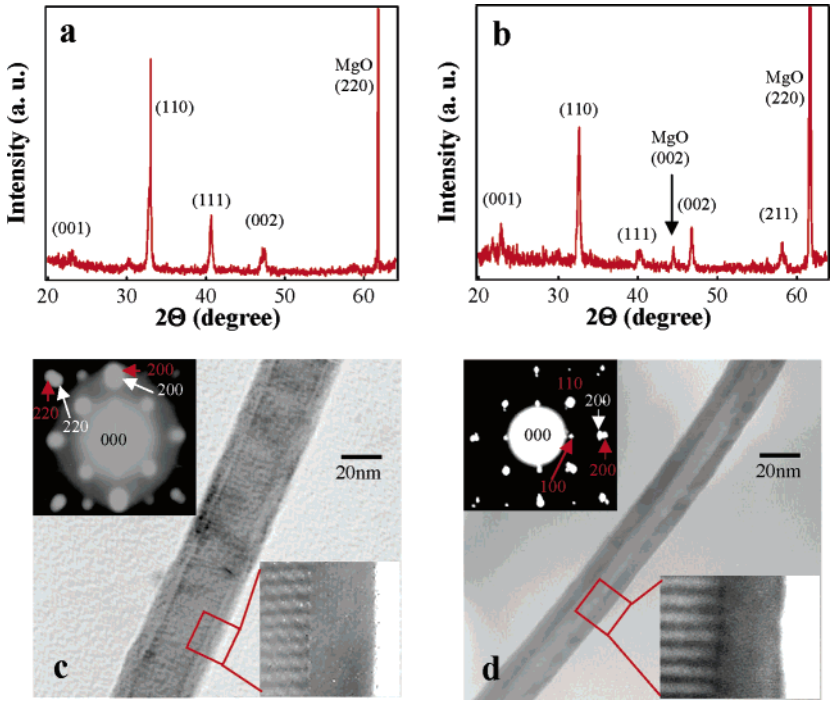

Figure 4. (a) XRD spectrum of the MgO/LCMO nanowire sample and (b) XRD spectrum of the MgO/LSMO nanowire sample grown on Si/SiO_2. (c) TEM image of an MgO/LCMO nanowire and (d) TEM image of an MgO/LSMO nanowire, both showing uniform shell layer coating. The boxed regions of panels c and d are shown in the respective lower right insets at higher magnification. Upper left insets of panels c and d: SAED patterns for MgO/LCMO and MgO/LSMO core−shell nanowires, respectively.

normal to the substrates (Figure 2b), consistent with our previous paper.[5] Synthesizing these vertical MgO nanowires, however, requires the use of expensive single-crystalline MgO substrates. It is therefore highly desirable to develop an efficient route to produce high-quality manganite nanowires on readily available substrates, such as Si/SiO_2 wafers. To achieve this, we first synthesized MgO nanowires atop Si/SiO_2 substrates by using gold clusters as the catalyst and Mg_3N_4 as the feedstock, using a method adapted from our previous publication.[5] Figure 2c displays a top view SEM image of the as-grown MgO nanowires. These nanowires appear to be lying on the substrate and follow random orientations, in sharp contrast to the vertically aligned MgO nanowires in Figure 2a. Surprisingly, a perspective view (Figure 2d) of the sample reveals that the MgO nanowires are actually standing on the Si/SiO_2 substrate at various angles. These nanowires could therefore work as good templates for the subsequent pulsed laser deposition to produce the desired core−shell nanowires.

Figure 2e displays a SEM image of the randomly oriented nanowires after LCMO coating. The deposited layer appears rather smooth, as shown in the Figure 2e inset. The smooth and uniform coating has also been observed in a similar experiment performed on randomly oriented MgO/LSMO nanowires, with the images shown in Figure 2f. The homogeneous epitaxial growth is truly remarkable and noteworthy, as the randomly oriented nanowires are likely exposed to the highly directed laser ablation plumes from one direction. In fact, such a shadow effect has resulted in nanotape heterostructures due to the selective deposition on one side of the nanoribbon substrates.[4] Inspired by the anisotropic growth kinetics proposed by Wang,[34] we tentatively attribute the homogeneous epitaxial growth to the migration of the deposited atomic species on the cylindrical nanowire surfaces. Namely, at very high temperatures, newly deposited atoms (or ions) with sufficient mobility can move freely on the nanowire surface and form a homogeneous layer (if under optimized condition) instead of being stuck at their landing positions. However, on the surface of nanobelts or nanoribbons, the atom mobility is insufficient to enable hopping between adjacent facets; therefore, the deposition is confined in a single surface, as has been observed in previous studies.[4] Our successful homogeneous growth of LCMO and LSMO on randomly oriented cylindrical MgO nanowires eliminates the necessity of the vertically aligned nanowire template, which relies on epitaxial growth on very limited single crystalline substrates. Therefore, our discovery greatly expands the diversity of the template materials for the synthesis of 1-D heterostructures.

More precisely, homogeneous coating on the randomly oriented nanowire surfaces was only formed under optimized growth conditions including laser power, temperature, pressure, gas flow rate, and the target-to-substrate distance. We realized that the plume generated by the laser beam is one of the major factors affecting the epitaxial growth of manganites. The visible plume is under the influence of both beam power density and O_2 pressure. The beam power density determines the initial plume energy that defines the mean free path L_0 of the plasma particles, namely, how far the plume can travel before scattering-induced thermalization. Not surprisingly, the target-to-substrate separation D also plays a critical role in the PLD process, which has been revealed in previous studies on the epitaxial growth of YBCO thin films.[15] The optimum distance in our case was found to be 2 cm $< D <$ 3 cm (Figure 3b), while samples off this position got either a very rough coating at $D = \sim 0.5$ cm (Figure 3a) or insufficient coating at $D = \sim 4$ cm (Figure 3c).

To verify the composition of the randomly orientated core−shell nanowires, we have used X-ray diffraction (XRD) to inspect the final products. Figure 4a,b shows the XRD spectra obtained from MgO/LCMO and MgO/LSMO nanowire samples, in which the peaks from MgO are well-separated from those of LAMO due to the lattice mismatch (9%) between the two materials. The two primary peaks originated from LAMO (110) and MgO (220) indicate the single crystallinity of both core

and shell materials. To examine their detailed morphology, we have further investigated the core−shell nanowires with transmission electron microscopy (TEM). Figure 4c shows a typical TEM image taken with an individual MgO/LCMO nanowire. The core diameter and shell thickness were measured to be 30 and 10 nm, respectively. Clear moiré fringes are visible in the inner region of the core−shell nanowire (lower right inset), where the overlapping MgO and LCMO lattices lead to the periodic beating-like pattern.[5] The single crystallinity of the conformal LCMO coating was further revealed by the high-resolution (HR) TEM image shown in the lower right inset of Figure 4c. The moiré fringes are parallel to the LCMO (100) plane and normal to the axial direction of the core−shell nanowire. This reveals that the axial direction of the supporting core is along [100], which is consistent with our previous study.[5] The upper left inset of Figure 4c shows the [001] zone axis selected area electron diffraction (SAED) pattern of the MgO/LCMO core−shell nanowire. The diffraction spots coming from the LCMO shell and MgO core were indexed with red and white numbers, respectively. This SAED further confirms the good epitaxial growth. Similarly, we have performed TEM, HRTEM, and SAED inspections on MgO/LSMO core−shell nanowires, with the images shown in Figure 4d and its insets. The pulsed laser deposition of LSMO was carried out in a way very similar to the LCMO deposition, except that different oxygen pressures were used during the deposition (200 mTorr for LCMO and 350 mTorr for LSMO). By tuning the deposition time, we can obtain a LSMO coating ~10 nm, as shown in Figure 4d. The core diameter for most of the nanowires falls within 10 nm (Figure 4d) and 30 nm (Figure 4c). This finite distribution is a direct result of the gold catalyst size distribution and the migration and aggregation of the catalyst particles when heated for the MgO nanowire growth. The previous material characterizations clearly demonstrate the good quality of the conformal manganite coating on the randomly oriented MgO nanowires.

These high-crystalline MgO/Manganite core−shell nanowires provide us with an ideal platform to study the electron transport through quasi-1-D channels of CMR materials. This ideal model would help to simplify the complex physics system and narrow the gap between a real system and a theoretical model in such a complicated CMR system. To extract the real signal from the material itself instead of electrical contacts, transport studies were carried out by measuring the four-probe resistance of individual core−shell nanowires. To pattern the four-probe metal electrodes, we first sonicated the core−shell nanowrie off the Si/SiO_2 substrate into 1-isopropanol and then dispersed the nanowire suspension onto another Si/SiO_2 substrate with preformed large electrodes. SEM inspection was employed to determine the location of the nanowires, and then e-beam lithography was used to pattern the contact electrodes perpendicular to the nanowires, followed by deposition of the Ag/Au electrodes. This method guaranteed that only one nanowire would be contacted by a group of electrodes, and multiple nanowire devices could be made on one chip. Figure 5a shows the SEM image of a typical device with a 5 μm long nanowire and four uniformly distributed electrodes. TEM studies performed with the nanowires left in the 2-propanol solution revealed that the MgO core is ~20 nm in diameter and that the shell layer is ~10 nm in thickness for both LCMO and LSMO. The four-probe resistance of an MgO/LCMO nanowire was recorded as a function of temperature under two different magnetic fields (0 and 1 T), as shown in Figure 5b. There exists a broad cusp that separates two regions showing semiconducting and metallic behaviors. This metal-to-insulator (MIT) transition

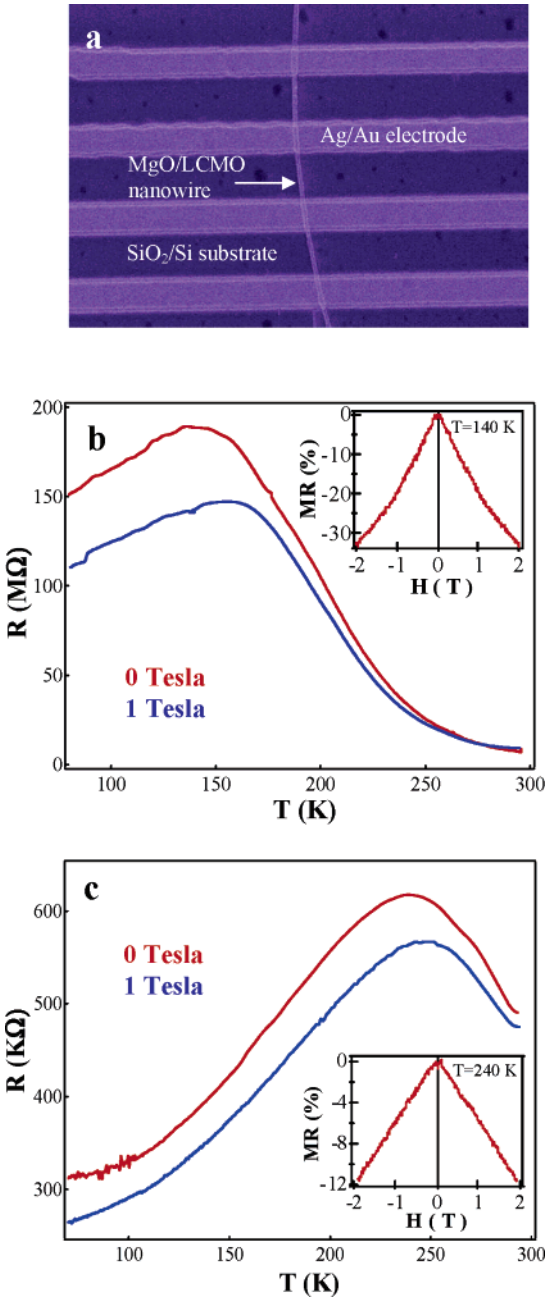

Figure 5. (a) Top view SEM image of a core−shell nanowire device showing four Ag/Au contact electrodes with even spacing. (b and c) Four-probe resistance (R) vs temperature (T) curves taken at two different magnetic fields $B = 0$ T (red) and B = 1 T (blue), with a MgO/LCMO nanowire (b) and a MgO/LSMO nanowire (c). Insets of panels b and c: magnetoresistance (MR) recorded at temperature $T =$ 140 K for panel b and $T = 240$ K for panel c, respectively.

occurred at ~140 K under zero magnetic field, and the transition temperature (T_{MIT}) shifted to ~160 K when a magnetic field of 1 T was applied normal to the device substrate. This MIT transition and T_{MIT} shift effect induced by magnetic fields strongly suggests a correlation between the ferromagnetism and the metallicity, which has been attributed to the double-exchange mechanism.[35−37] When temperature is lowered, the system consisting of the hopping electrons (itinerant) and local moments would lower its total energy by aligning the spins ferromagnetically and allowing itinerant electrons to gain kinetic energy. Namely, the spin-polarized electrons move freely in the whole crystal with enough kinetic energy once the spin fluctuation is sufficiently suppressed by lowering the temperature or applying

a magnetic field, and thus, the transition occurs. This MIT associated with ferromagnetic to paramagnetic transition also happened in MgO/LSMO core−shell nanowires with $T_{MIT} = \sim 240$ K at $H = 0$ and the T_{MIT} shifted to ~250 K under a perpendicular magnetic field of 1 T (Figure 5c). In addition, MR measurements were also performed with both MgO/LCMO (inset of Figure 5b) and MgO/LSMO (inset of Figure 5c) core−shell nanowires at their transition temperature by sweeping the perpendicular magnetic field between ±2.0 T. By defining the MR ratio as $[R(H) - R(0)]/R(0) \times 100\%$, a value of 34% is achieved at $T = 140$ K and $H = 2.0$ T for LCMO (inset of Figure 5b), and 12% is achieved at $T = 240$ K and $H = 2.0$ T for LSMO (inset of Figure 5c).[38] No saturation has been observed in either of the core−shell nanowires, indicating the nature of the CMR effect. We note that the device resistance for both LCMO and LSMO nanowires has a wide distribution, sometimes up to 1 order of magnitude. More in-depth work is necessary to gain stringent control over the nanowire synthesis and the device fabrication process.

In summary, we have successfully synthesized high-crystalline MgO/LCMO and MgO/LSMO core−shell nanowires based on randomly oriented MgO nanowire templates using the PLD method. The surprising success in producing homogeneous coating on randomly oriented nanowires could be attributed to the migration of surface atoms/ions. We also found the epitaxial growth of manganite sensitively depends on several synthesis parameters including temperature, pressure, laser power, and sample−target separation, etc. In particular, the sample−target distance and the MgO nanowire density play the most critical roles in determining the quality of the final products. Following a series of material characterizations, we have further investigated the electronic transport behavior and MR properties of these 1-D manganite nanowires. Remarkable MIT transition and CMR effect have been observed in both LCMO and LSMO nanoscale systems.

Acknowledgment. We thank Dr. Nanfeng Zhang for his help with the XRD characterizations. We gratefully acknowledge support from a NSF CAREER Award, a NSF-CENS grant, and a SRC MARCO/DARPA grant.

References and Notes

(1) Gudiksen, M. S.; Lauhon, L. J.; Wang, J.; Smith, D. C.; Lieber, C. M. *Nature* **2002**, *420*, 57.

(2) Chang, K. W.; Wu, J. *J. Adv. Mater.* **2005**, *17*, 241.

(3) Suenaga, K.; Colliex, C.; Demoncy, N.; Loiseau, A.; Pascard, H.; Willaime, F. *Science* **1998**, *278*, 652.

(4) He, R. R.; Law, M.; Fan, R.; Kim, F.; Yang, P. D. *Nano Lett.* **2002**, *2*, 1109.

(5) Han, S.; Li, C.; Liu, Z. Q.; Lei, B.; Zhang, D. H.; Jin, W.; Liu, X. L.; Tang, T.; Zhou, C. W. *Nano Lett.* **2004**, *4*, 1241.

(6) Zhang, D. H.; Liu, Z. Q.; Han, S.; Li, C.; Lei, B.; Stewart, M. P.; Tour, J. T.; Zhou, C. W. *Nano Lett.* **2004**, *4*, 2151.

(7) Fu, L.; Liu, Z. M.; Liu, Y. Q.; Han, B. X.; Wang, J. Q.; Hu, P. G.; Cao, L. C.; Zhu, D. B. *J. Phys. Chem. B* **2004**, *108*, 13074.

(8) Jiang, X. C.; Mayers, B.; Herricks, T.; Xia, Y. N. *Adv. Mater.* **2003**, *15*, 1740.

(9) Manna, L.; Scher, E. C.; Li, L. S.; Alivisatos, A. P. *J. Am. Chem. Soc.* **2002**, *124*, 7136.

(10) Obare, S. O.; Jana, N. R.; Murphy, C. J. *Nano Lett.* **2001**, *1*, 601.

(11) Kong, X. Y.; Ding, Y.; Wang, Z. L. *J. Phys. Chem. B* **2004**, *108*, 570.

(12) Fu, X. L.; Ma, Y. J.; Li, P. G.; Chen, L. M.; Tang, W. H.; Wang, X.; Li, L. H. *Appl. Phys. Lett.* **2005**, *86*, 143102.

(13) Hu, J. Q.; Bando, Y.; Liu, Z. W.; Sekiguchi, T.; Golberg, D.; Zhan, J. H. *J. Am. Chem. Soc.* **2003**, *125*, 11306.

(14) Li, Q.; Wang, C. R. *J. Am. Chem. Soc.* **2003**, *125*, 9892.

(15) Geohegan, D. B. *Thin Solid Films* **1992**, *220*, 138.

(16) Zheng, J. P.; Ying, Q. Y.; Witanachchi, S.; Huang, Z. Q.; Shaw, D. T.; Kwok, H. S. *Appl. Phys. Lett.* **1989**, *54*, 954.

(17) Gupta, A.; Hussey, B. W.; Kussmaui, A.; Segmuller, A. *Appl. Phys. Lett.* **1990**, *57*, 2365.

(18) Girault, C.; Damiani, D.; Aubreton, J.; Catherinot, A. *Appl. Phys. Lett*. **1989**, *55*, 182.

(19) Dyer, P. E.; Issa, A.; Key, P. H. *Appl. Phys. Lett*. **1990**, *57*, 186.

(20) Jin, S.; Tiefel, J. H.; McCormack, M.; Fastnacht, R. A.; Ramesh, R.; Chen, L. H. *Science* **1994**, *264*, 413.

(21) Haghiri-Gosnet, A.-M.; Renard, J.-P. *J. Phys. D: Appl. Phys.* **2003**, *36*, R127.

(22) Ramirez, A. P. *J. Phys. Condens. Matter* **1997**, *9*, 8171.

(23) Schiffer, P.; Ramirez, A. P.; Bao, W.; Cheong, S.-W. *Phys. Rev. Lett.* **1995**, *75*, 3336.

(24) Maezono, R.; Ishihara, S.; Nagaosa, N. *Phys. Rev. B* **1998**, *58*, 11583.

(25) Jin, S.; McCormack, M.; Tiefel, T. H.; Ramesh, R. *J. Appl. Phys.* **1994**, *76*, 6929.

(26) Derbyshire, K.; Korczynski, E. *Semicond. Sci. Technol.* **1995**, *38*, 57.

(27) Rajeswari, M.; Goyal, A.; Shreekaka, R.; Lofland, S. E.; Bhagat, S. M.; Boettcher, T.; Kwon, C.; Ramesh, R.; Venkatesan, T. *Appl. Phys. Lett.* **1996**, *69*, 851.

(28) Xiang, Z. H.; Wu, D.; Vardeny, Z. V.; Shi, J. *Nature* **2004**, *427*, 821.

(29) Kumar, D.; Sankar, J.; Narayan, J.; Rajiv; Singh, K.; Majumdar, A. K. *Phys. Rev. B* **2002**, *65*, 094407.

(30) Urushibara, A.; Moritomo, Y.; Arima, T.; Asamitsu, A.; Kido, G.; Tokura, Y. *Phys. Rev. B* **1995**, *51*, 14103.

(31) Lu, C. J.; Wang, Z. L.; Kwon, C.; Jia, Q. X. *J. Appl. Phys.* **2000**, *88*, 4033.

(32) Ma, X. Y.; Zhang, H.; Xu, J.; Niu, J. J.; Yang, Q.; Sha, J.; Yang, D. R. *Chem. Phys. Lett.* **2002**, *363*, 579.

(33) Urban, J. J.; Lian, O. Y.; Jo, M.-H.; Wang, D. S.; Park, H. K. *Nano Lett.* **2004**, *4*, 1547.

(34) Wang, Z. L. *Annu. Rev. Phys. Chem.* **2004**, *55*, 159.

(35) Zener, C. *Phys. Rev.* **1995**, *81*, 440.

(36) Anderson, P. W.; Hasegawa, H. *Phys. Rev.* **1995**, *100*, 675.

(37) De Gennes, P. G. *Phys. Rev.* **1960**, *118*, 141.

(38) We note that a slightly different definition was used in our previous publication (ref 5): $MR = [R(H) - R(2T)]/R(2T) \times 100\%$. Both ways of defining magnetoresistance are common practice and can be found in the literature.